Research Article

Preparation and characterization of cellulose nanocrystals with different aspect ratios as nano-composite membrane for cationic dye removal

Duo Liu[1,2] · Jie Liu[1,2] · Song Lin[2] · Xiaohui Wei[2] · Min-jie Guo[1]

Received: 13 April 2019 / Accepted: 8 November 2019 / Published online: 11 November 2019

Abstract
Two cellulose nanocrystals (CNCs) with different aspect ratios in dimension derived from raw microcrystalline cellulose were prepared and presented in this paper. The morphological features of nanostructures were explored with TEM. Then the structure analysis, surface charge and thermal degradation behavior of CNCs were characterized and determined by FTIR/X-ray diffraction, zeta potential and TGA, respectively. Furthermore, the hybrid CNCs nano-composite membranes were facilely fabricated via vacuum-dewatered process for effective removal of cationic dyes (up to 99.9% removal of methylene blue at 10 mg/L and 97.9% removal of rhodamine B at 20 mg/L). The mechanism of such effective cationic dye removal is derived from the combined effect of both electrostatic interaction and steric hindrance between the CNC composite membrane and the cationic dyes during the filtration process. In addition, the permeation flux and dye removal efficacy of the composite membrane are CNCs loading-concentration dependent.

Keywords Cellulose nanocrystals · Aspect ratio · Dye removal · Composite membrane

1 Introduction

Cellulose nanocrystals (CNCs) are renewable and eco-friendly materials that maintain the basic structures of cellulose, but possess many special characteristics such as large specific surface area, high crystallinity, high specific modulus and strength, and low cost [1, 2]. Therefore, CNCs have been widely utilized as a reinforcement additive of vast nanocomposite materials, tissue engineering scaffolds, drug carriers, separators, flocculants, and adsorbents [3–5].

In general, various approaches have been applied to prepare the CNC samples, i.e. acid hydrolysis via individual or combined sulfuric acid, hydrochloric acid or acetic acid under ultrasonic or microwave irradiation [6–8], 2,2,6,6-tetramethyl-piperidine-1-oxyl (TEMPO) mediated-oxidation [9], ammonium persulfate (APS) oxidation [10], enzymatic hydrolysis [11], and physical ball-milling [12].

Meanwhile, the sources of CNCs are also abundant originated from diverse bacterial, cotton, microcrystalline cellulose (MCC), ramie, tunicate, and wood [13]. Despite so many methods in preparing the CNCs, little attention has been paid to their dimension difference, especially the aspect ratio (AR) factor of influence for their application. Normally, the dimension of CNCs is approximately a few nanometers in width, but from tens of nanometers to several micrometers in length. The AR, defined as the

Electronic supplementary material The online version of this article (https://doi.org/10.1007/s42452-019-1654-2) contains supplementary material, which is available to authorized users.

✉ Song Lin, lynchpku@163.com; ✉ Min-jie Guo, guomj@tust.edu.cn | [1]College of Chemical Engineering and Materials Science, Tianjin University of Science and Technology, Tianjin 300457, China. [2]Institute of Medical Support, Academy of Military Sciences, Tianjin 300161, China.

length-to-width (L/W value) spans a very broad range window. In general, higher AR of CNCs contributes to a better reinforcing effect, resulting in improved mechanical properties [14].

Sun et al. [15] reported the transparent cellulose films from CNC but with two distinct aspect ratios. It was found that the films made from larger aspect ratio exhibited higher optical transmittance and larger tensile strength, while the one from smaller aspect ratio showed better thermal stability, higher crystallinity and lower coefficient of thermal expansion. However, the two individual samples were obtained via different preparation methods from the same bleached wood pulp, by converting the hydroxymethyl groups on their side chain to the either carboxylic [16, 17] or sulfate forms [18], respectively. Thus, it is hard to tell whether the aspect ratio is the key influence factor to the final properties of CNC nanopapers. Kalashnikova et al. [19] studied cellulosic colloidal nanorods with various aspect ratios at the oil–water interface for Pickering emulsion, but the raw materials are derived from different origins.

Currently, textile dyes are the most important worldwide pollutant source in water [20]. The increasing of dye pollutants in water is extremely hazardous to the plant, animal and human life [21]. Sometimes it is difficult to treat the dye pollutants in water since they have stable and diverse molecular structures which makes them more difficult to be biodegraded [22]. Therefore, solving this water pollution issue by removing the dye contaminants with low-cost adsorbents is a major concern that benefits the environmental remediation [23, 24].

Membrane separation and filtration technology has been a promising technology with lower energy cost to separate substances from a mixture by filtering that mixture through a porous membrane [25]. Nanofiltration (NF), a pressure-driven membrane separation process, has practical applications in water treatment for rejection of salts and dyes [26]. The mechanism is based on the steric hindrance (sieving) effect and electrostatic interaction (Donnan) effects [27]. The main drawbacks of membrane filtration are relatively short membrane life which limited their application for treating dye wastewater [28].

Cellulose acetate (CA) is a commonly used membrane material for both ultrafiltration (UF) and reverse osmosis (RO) filtration [29]. It is served as one of the ideal polymer matrix candidate in fabricating membranes due to its renewable characteristics, long-term good mechanical strength as well as the superior film-forming ability. However, one drawback of CA membranes is the lack of reactive functional groups on the polymer backbones to enhance the separation efficiency of the membranes.

In this work, we firstly assessed the effect of preparation conditions on morphological, crystalline, and thermal behavior of CNC from the same raw resource, i.e. MCC, to exploit their potential application as nanocomposites membrane for dyes removal. In order to eliminate the discrepancy of residual modified groups on the final CNC products, the sulfuric acid, a well-known agent used to remove amorphous regions of cellulose, was applied as the only hydrolytic media during the entire preparation process. Finally, the nanocomposite membrane of CNC was conducted through vacuum dewatering process onto a sheet of mixed CA (MCA) membrane and further used for effective dye removal of three kinds of dyes, i.e. methylene blue (MB), methyl orange (MO) and rhodamine B (RhB). The MB and RhB are used as model cationic dyes for wastewater treatment, while the MO shows negative charges in neutral solution due to its sulfuric groups.

2 Experimental

2.1 Materials and methods

Micro-crystalline cellulose (MCC) 25 μm (order item No. C104843, denoted as MCC-25) and 250 μm (order item No. C104844, denoted as MCC-250) were purchased from Aladdin Chemical Co., Ltd. (Shanghai, China). Concentrated sulfuric acid (98%) was obtained from Tianjin Chemical Reagent Co., Ltd. Methylene blue (≥ 98.5%), methyl orange (AR), rhodamine B (AR) were supplied by Tianjin Dingguo chemicals, Tianjin Kermel chemicals and Tianjin Yingda Rare chemicals, respectively. The mixed cellulose acetate (MCA, 50 mm in diameter, 0.22 μm in pore size) membranes was obtained from Shanghai Xinya scavenging material plant.

The particle size distribution of raw MCC was measured by laser granulometry using Mastersizer 3000 (Malvern). The microstructure and morphology of the MCC and CNC and corresponding composite samples were analyzed by transmission electron microscopy (TEM, 2010FEF, Japan Electronics Co., Ltd.) at 200 kV and atomic force microscopy (AFM, asylum research AFM Cyphers, Oxford Instruments). The AFM imaging was performed in a Multimode AFM with ARC SPM controller. All images were recorded in AC mode (peak force tapping mode) at room temperature in air. The AFM tips of spring constant value 0.4 N/m was purchased from ASYLUM AFM probes. Meanwhile the modulus, mechanical strength of the crystals and surface roughness of composite membranes was measured by AFM. To further evaluate the CNC dimension,

an image analysis software (Image J) was utilized to analyze the size of CNC with randomly 50 counts of each sample in TEM images. The crystalline patterns were evaluated by means of a wide-angle polycrystalline X-ray diffractometer (XRD, D8 Advance, Bruker Technology, Germany). FTIR absorption spectra were recorded on a fourier transform infrared spectrometer (NICOLET 6700, Thermo Fisher Scientific Technology Co., Ltd). The measurements were carried out over the 400–4000 cm^{-1} range at room temperature. The scan number was 32 per spectrum with the spectral resolution of 4 cm^{-1}. The ZETA potential was measured by the Nano-90 (Malvern). The thermal behavior of CNC was studied using a thermogravimetric analyzer (TGA-50, Shimadzu, Japan) in N_2 at a heating rate of 10 °C/min from 100 to 700 °C. UV spectra of dyes solution before and after filtration were detected on Shimadzu-1700 from 400 to 800 nm. Scanning electron microscopy (SEM, JSM-6700F, JEOL) at 10 kV was used to examine the surficial and internal composite membrane micro-structures. For the cross-sectional view of the membranes, they were firstly dipped into liquid N_2 to become fragile and freshly cut to produce the cross-sectional interface for SEM observation. Meantime, Elemental mapping of C, H, O, and S was performed on Vario MACRO cube, Element.

2.2 Preparation of CNCs

CNC was prepared by following method under the ice-bath condition: in brief, 10 g of microcrystalline cellulose (MCC 25 µm or 250 µm) was mixed with 34.7 g of deionized (DI) water, then the pre-cooled 65.3 g of concentrated sulfuric acid (98%) at 0 °C was added dropwise slowly within 30 min under ice bath to avoid overheating of the mixed solution. The reaction was then transferred to perform at 45 °C for 2 h with constant stirring. The reaction was then halted by adding a tenfold excess of cold DI water. After standing overnight at 4 °C, the raw product of CNC was well precipitated and the supernatant water was decanted away. Then the settled sedimentation was collected and washed by centrifugation for 10 min at 9000 rpm/5 °C for three repeated cycles and dialyzed against DI water for at least 48 h using regenerated cellulose dialysis bags (molecular weight cut off = 12,000–14,000) until the pH of the solution reached neutral. Sonication was performed on the neutral CNC solution for 15 min under an ultrasonic processor (JY92-II, Ningbo Scientz, China) while immersed in an ice bath to obtain uniform solution and finally lyophilized to obtain solid CNC products, denoted as CNC-25f and CNC-250f, respectively for further characterizations and tests.

2.3 Fabrication of nano-composite membrane and dye-removal tests

The fixed 3.0 mL of as-prepared dispersed CNC-25f (10.5 mg/mL) or CNC-250f (0.35 mg/mL, 1.06 mg/mL, 3.53 mg/mL, and 10.6 mg/mL) solution was vacuum-dewatered onto an individual sheet of commercial MCA membranes as support substrate, respectively. The overall bulk density of CNC-25f@10.5 and CNC-250f@10.6 is 0.402 g/cm^3 and 0.406 g/cm^3, respectively (Table S1). Then the CNC solution was left to dewater through vacuum pump until a deposited layer of CNC was clearly observed on the surface of the membrane. Then 5 mL of three kinds of dyes, i.e. methylene blue (MB, 10 mg/L), methyl orange (MO, 10 mg/L), Rhodamine B (RhB, 20 mg/L) solution was dropwise added onto the thus obtained nano-composite membrane sheets and pump vacuumed for filtration. The filtrate of the dye solution before and after was monitored by UV spectra and the removal percentage of dyes was calculated according to the following Eq. (1).

$$\text{Removal}\,\% = \left(A_0 - A_1\right)/A_0 \times 100\% \quad (1)$$

where A_0 is the λ_{max} absorbance intensity of each dye at initial concentration and A_1 is the λ_{max} absorbance intensity of each dye after filtration. (λ_{max} = 664 nm for MB, λ_{max} = 464 nm for MO, λ_{max} = 554 nm for RhB).

The membrane performance of permeation flux was determined by MB solution (10 mg/L) for each as-prepared membrane under certain operation pressure at 25 °C. And the factor Flux (F) was calculated by Eq. (2):

$$F = V/(A \times t) \quad (2)$$

where *F* (L/m^2/h) is the flux, *A* (m^2) is the effective area of the membrane; *V* (L) is the volume of permeated MB solution through the membrane during the time *t* (h).

3 Results and discussion

One of the common processes for the isolation of CNC from cellulose fibers is based on acid hydrolysis. The disordered or para-crystalline regions of cellulose are more preferentially hydrolyzed to acid attack, whereas the crystalline regions can remain intact due to their rigid structure with higher acid resistance [30]. Therefore, after an acid treatment, the amorphous regions of cellulose were removed, and the rod-like CNCs are produced. As shown in TEM images, the raw MCCs are amorphous fibril networks in morphology (Fig. 1a, c). After the acid treatment

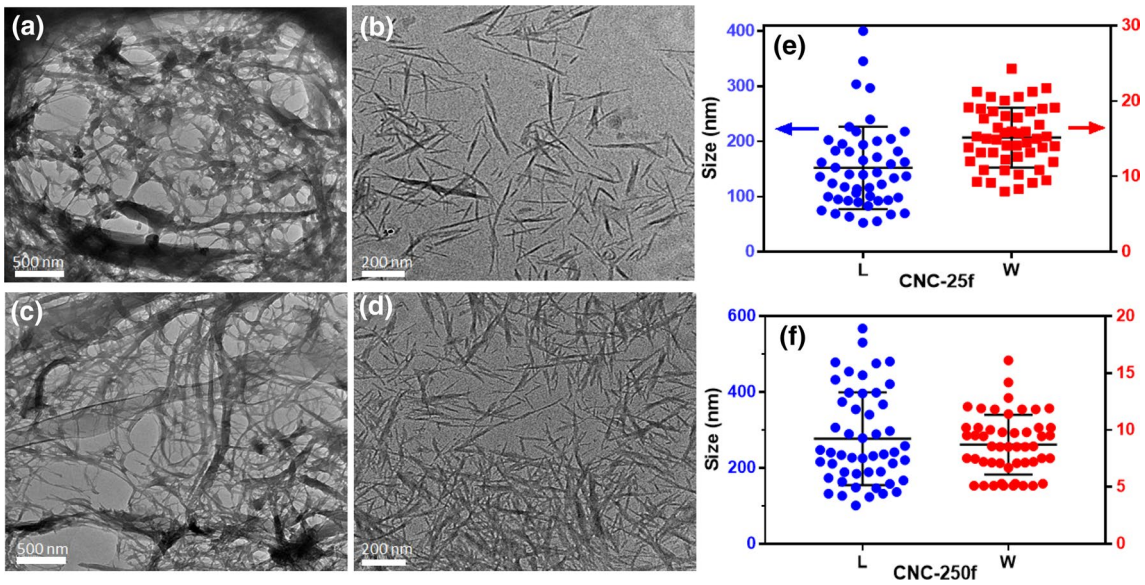

Fig. 1 TEM images of each sample. **a** MCC-25, **b** CNC-25f, **c** MCC-250, **d** CNC-250f. Size distribution (Length (L) × Width (W)) of as prepared CNC samples, **e** CNC-25f, **f** CNC-250f (n = 50 counts)

of cellulose in this study can successfully produce rod-like cellulose nanocrystals. The micron-size scale of raw material MCC are shown in Table S2, where the Dv(50) value is 15.9 µm and 210.1 µm for MCC-25 and MCC-250, respectively. Since the size scale of raw MCC-25 and MCC-250 is 25 µm and 250 µm according to the supplier's order information, it is believed that the Dv(50) values matches closer to its commercial description.

The morphology of obtained CNC is nano-whiskers as similar as reported previously [31]. After a statistical examination, it was found that the geometry of the two CNCs are quite different, i.e. length (L), width (W) and corresponding AR values. Detailed results are shown in Fig. 1e, f and Table S3. For instance, the CNC length obtained by 25 µm of MCC (MCC25) is distributed around 150 nm (CNC-25f, Fig. 1e), while for the CNC-250f is ca. 280 nm (Fig. 1f). After statistically calculation, the distinct AR values of CNC-25f and CNC-250f are 10.7 ± 5.9 and 34.8 ± 18.2, respectively (Table S3).

As seen from Fig. 2a, all the hydrolyzed CNC samples exhibited a typical cellulose I type crystalline structure [8, 32, 33], with no traces of a mixed lattice type as indicated by the XRD peaks in the diffractogram located at approximately 14.9°, 16.3°, 22.5° and 34.6° (2θ), which corresponds to (1$\bar{1}$0), (110), (200) and (004) reflection planes, respectively [15, 34]. The FTIR spectra of the MCCs and obtained CNCs are shown in Fig. 2b. The characteristic spectra of both the CNC samples were similar, but slightly different from that of original MCC from 400 to 4000 cm^{-1}, indicating the basic cellulose structures remain the same after the acid treatment. The broad band ranging from 3000 to 3750 cm^{-1} region is assigned to O–H stretching vibrations, the band at 2910 cm^{-1} to C–H stretching vibrations, and 1384 cm^{-1} to the C–O–H deformation vibration [35]. Compared with the corresponding MCCs, the CNCs exhibited increases in the intensities of the bands at 1055 and 1110 cm^{-1} assigned to the C–O–C stretching of pyranose and glucose ring skeletal vibration, respectively, which implies the increase of the crystalline cellulose content in CNCs [36]. Moreover, the minor peaks at 709 cm^{-1} and 3270 cm^{-1} assigned to the O–H out-of-plane bending and the O–H stretching for native cellulose Iβ structures [37]. It is also worth noting that a new minor peak at 1205 cm^{-1} assigned to S=O stretching from sulfate groups appeared in the CNC samples, indicating the success of hydrolyzing cellulose with sulfuric acid to form esterification with the hydroxyl groups during acid hydrolysis. The broad peaks centered at 3420 cm^{-1} are the stretching vibration of the OH groups derived from cellulose [38].

Figure 3 illustrates the thermal properties, i.e. TGA (Fig. 3a) and DTG (Fig. 3b) curves of the prepared CNCs via different MCCs. It can be seen that cellulose nanocrystals obtained from different MCC sources show a similar trend in thermal behavior. At a relative low temperature of around 130 °C, the CNCs started a thermal degradation in TGA curves, and nearly 40% of mass were lost in the 130–240 °C region. With further increases of treated temperature up to 700 °C, further

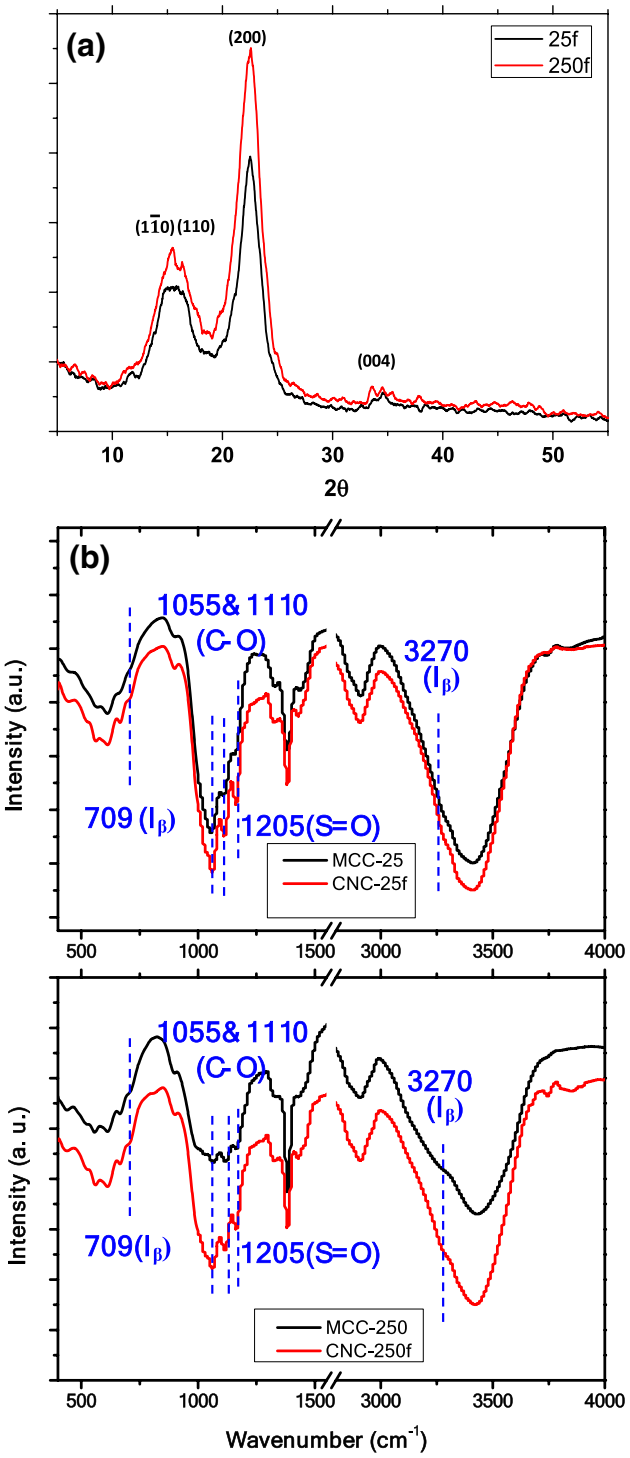

Fig. 2 **a** XRD patterns of as-prepared CNC-25f and CNC-250f samples, **b** FTIR spectra of commercial MCCs and the as-prepared CNCs

decomposition of CNCs occurred with ca. 40 wt% residues. However, the CNC-250f shows a bit faster thermal-decomposition property than CNC-25f. The differences in thermal behavior among these CNCs may be explained by the fact of the sulfuric acid hydrolysis [18]. The existence of surface sulfated groups would significantly lower the degradation temperature of CNCs due to the sulfated anhydroglucose elimination required less energy [39]. Thus, during the thermal degradation process, sulfuric acid molecules could be released at much lower temperatures [40]. Then, the released sulfuric acid would further facilitate the decomposition or depolymerization of cellulose by removing some of the hydroxyl groups either via a direct catalysis or an esterification mechanism. Since the amount of modified sulfate groups varied (Table S4), thus leading to different TG curves of the CNCs.

Furthermore, the CNC-25f and CNC-250f were used to prepare nano-composite membrane for dye removal (Fig. 4a). MB and RhB were used as models to test its filtration ability. As shown in Fig. 4b, c, the percentage of MB removal is very efficient up to 98.3% and 99.9% for the composite CNC-25f and CNC-250f nano-composite membrane, respectively, whilst the neat MCA membrane can only remove 39.2% of total MB. Interestingly, when comes to the RhB removal (Fig. 4d, e), the CNC-250f nano-composite membrane still shows a good candidate as high as ca. 98% of RhB removal after the filtration. However, only 66.9% and 56.8% of RhB can be removed after pass through the CNC-25f composite membrane.

To further investigate the concentration effect of CNC-250f in composite membrane for the MB removal, serial 0.35 mg/mL, 1.06 mg/mL, 3.53 mg/mL, and 10.6 mg/mL of CNC-250f batch solution with fixed volume (3 mL) was used to prepare composite membranes via same procedure and denoted as CNC-250f@0.35, CNC-250f@1.06, CNC-250f@3.53 and CNC-250f@10.6, respectively. The overall MB removal results are shown in Fig. 5a, b. The CNC-250f composite filter membrane showed obvious concentration-dependent effect for the MB dye removal. At lowest loading amount at 3 mL of 0.35 mg/mL CNC-250f (CNC-250f@0.35), only the 70.4% of total MB can be removed after filtration compared with 39.2% of neat MCA membrane (Fig. 5b). With further increasing loading contents of CNC-250f from 1.06 mg/mL to 10.6 mg/mL, the percentage of MB removal can be achieved to 97.2%, 98.9% and finally up to 99.9% (Fig. 5b), respectively. From typical images shown in Fig. 5c, the filtrate solution became clear after passing through CNC-250f@3.53 and CNC-250f@10.6 composite membranes, while the CNC-250f@0.35 and CNC-250f@1.06 treated samples still bear with some bluish color visually, indicating incomplete removal of MB dyes. Overall, all the CNC composite membrane samples show an improved dye removal capacity than the neat MCA membrane. Meantime, the saturated adsorption capacity of CNC-250f@10.6 mg/mL

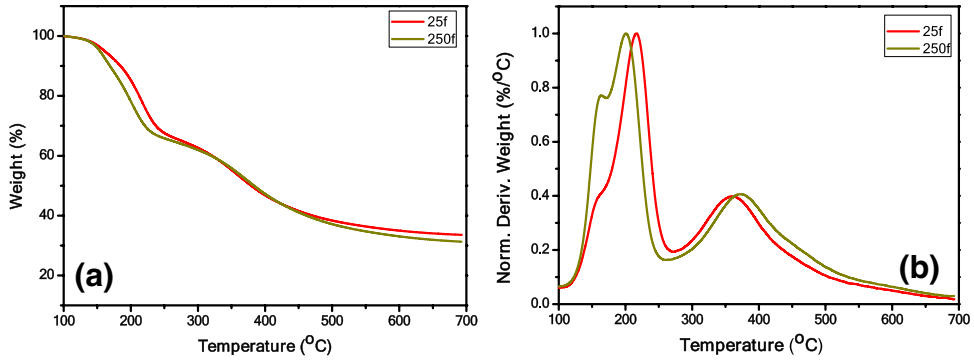

Fig. 3 TGA (**a**) and DTG (**b**) curves of the CNC-25f and CNC-250f

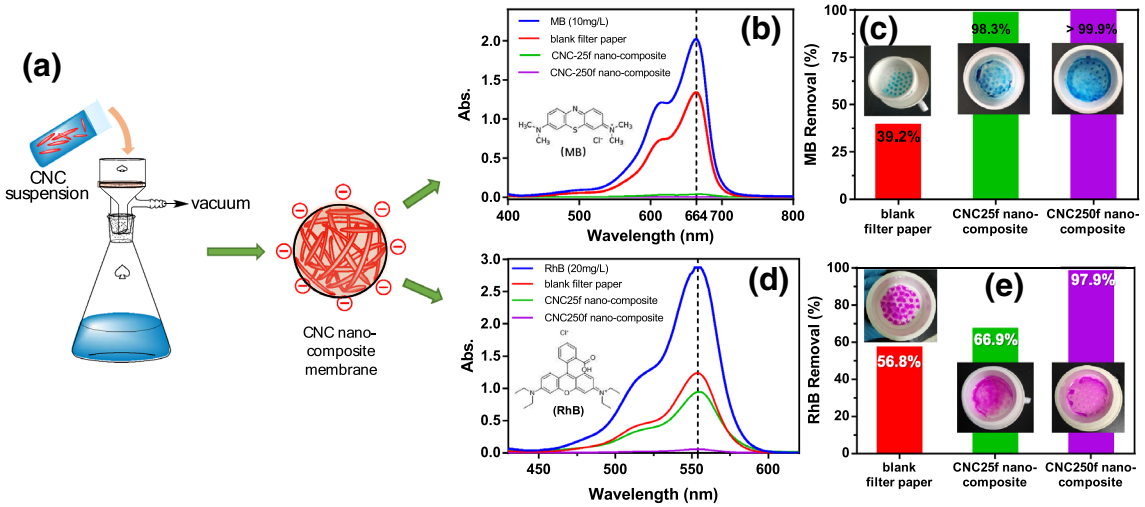

Fig. 4 **a** The schematic process of neat MCA and as-prepared CNC nano-composite membranes for selective MB (**b**, **c**) and RhB (**d**, **e**) removal monitored by UV spectra. Insets: Images of the filter membrane after removal of MB (**c**) and RhB (**e**)

nano-composite membrane was also determined (Fig. S1). It is revealed that such membrane can remove up to 99% of total 120 mL of MB filtrate@10 mg/L. Then the removal efficacy gradually declined to ca. 85% when another portion of 30 mL of MB filtrate@10 mg/L was added, indicating it's a good candidate when comes to treat a large amount of cationic dye pollutants in water.

These results could be mainly interpreted by steric hindrance, electrostatic adsorption and repulsion interaction between the CNC components and dye molecules. Firstly, surface roughness is a crucial factor to interfere with the effect of nanofiltration [41]. Thus, as determined by AFM (Fig. 6a–c), after a successful deposition of the CNC onto a MCA sheet, the surface morphology became much smoother compared to the neat MCA membrane. Further quantitative results are shown in Fig. 6d, the RMS (root-mean-squared) roughness were calculated with 17.6 ± 5.0 nm, 3.2 ± 0.4 nm, and 3.4 ± 0.4 nm for neat MCA membrane, CNC-25f, and CNC-250f composite membranes, respectively. The relatively smooth and compact stack composites contribute to the effective retention of dyes during the nanofiltration process. Secondly, the surface of composite membranes is negatively charged due to existence of the sulfate groups in the both the CNC-25f and CNC-250f with zeta potential values of − 59 mV and − 66 mV (Fig. 6e), respectively. The more negative surface charge of CNC-250f may be due to its relatively higher sulfate content (Table S4). Since the MB and RhB molecules are cationic in solution, they can be easily absorbed by the negatively charged CNC composite membranes through electrostatic interaction [42]. Thus, the CNC-250f nanocomposite membrane with more negatively charged surface results in an excellent and better cationic dye removal performance to both MB and RhB dyes. Such hypothesis can also be verified by another MO dye removal test, which is a negatively charged dye due to the benzene sulfonate

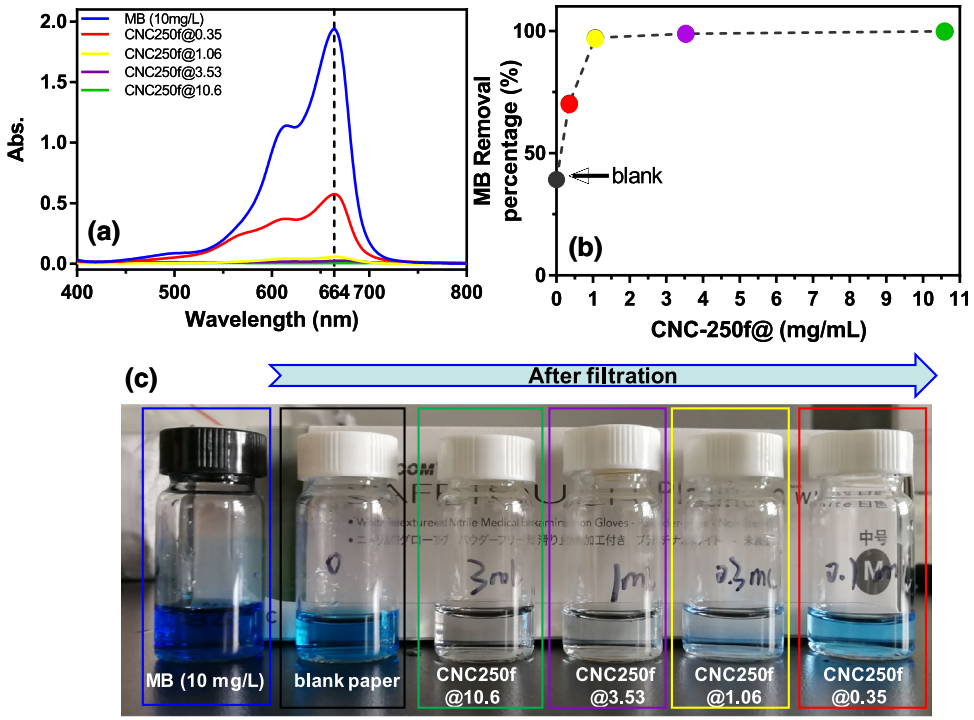

Fig. 5 Full UV spectra (**a**) and calculated percentage at λ_{max} = 664 nm of MB dye removal (**b**) with CNC-250f@0.35 (red), CNC-250f@1.06 (yellow), CNC-250f@3.53 (purple) and CNC-250f@10.6 (green), respectively. **c** Images of filtrate MB solution before and after pass through each individual composite filter membrane

groups in neutral solution. And after the same filtration process, it was found that the percentage of MO removal for all the membranes was relatively low, i.e. 42.2%, 50.9%, and 56.3% for MCA membrane, CNC-25f, and CNC-250f composite membranes, respectively (Fig. S2). This indicates that the strong electrostatic repulsive effect occurred between the CNC and MO dyes due to their same negative surface charge, thus leading to poor removal efficacy. In addition, the permeation flux (F) of composite membrane was also determined. For the neat MCA membranes, it showed relatively high flux at 60 L/m^2/h (Fig. 6f). Then the F values gradually decreased with the increasing loading contents of CNC-250f as the functional entities which serve as adsorbents in the composite membranes. The lowest F is ca. 12 L/m^2/h for the CNC-250f@10.6, indicating the strongest steric hindering effect as well as highest dye removal efficiency of the composite membranes.

Moreover, the surface and internal microstructures of these composite membranes were also explored by SEM. The top-view and cross-section morphologies of the membranes are shown in Fig. 7. The neat MCA membrane exhibited a random 3D porous microstructure with a fibrous network (Fig. 7a, b), in accordance to previous report [43]. When the cellulose nanocrystals (CNC-250f) were introduced to deposit onto the pristine MCA membrane, both components can be compatible with each other, and some agglomeration clusters at the interface was observed at relative low loading content (CNC-250f@1.06, Fig. 7c) compared with the neat MCA membrane (Fig. 7a) from the top-view due to the similar chemical structures between CNC and MCA. Nevertheless, some perforated sheets of cellulose nanocrystals are formed on the top layer of CNC composite membranes when higher CNC-250f contents, i.e. CNC-250f@3.53 and CNC-250f@10.6, were applied (Fig. 7e, g). Further cross-sectional examination of composite membranes can also detect some CNC self-aggregation knots or clusters within the bulk membranes (as dotted circle in insets of Fig. 7d, f, h). Higher loading content of CNC votes for more and larger CNC cluster aggregates, but overall the porous structures are still maintained favoring for the pass through of water during the dye removal test as shown in Figs. 4, 5, Fig. S1 and Fig. S2.

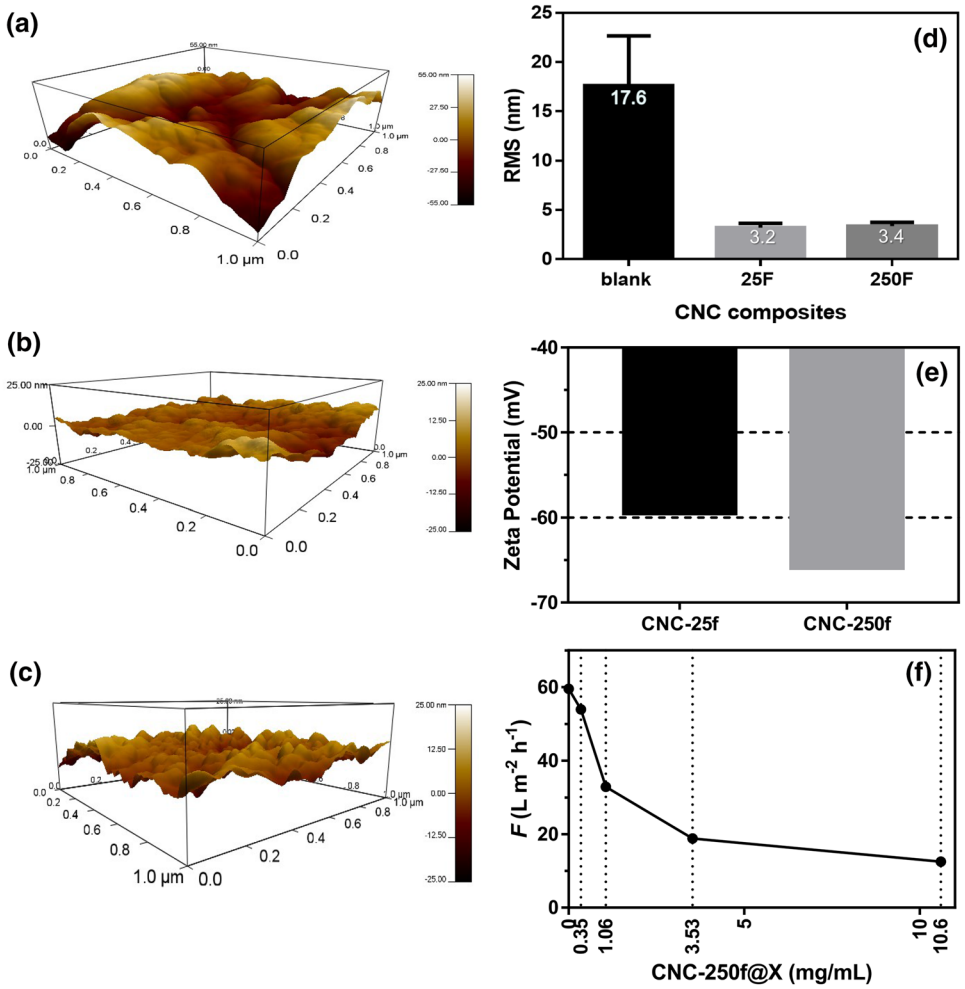

Fig. 6 3D tapping mode of AFM surface images (1×1 μm^2): **a** blank MCA membrane, **b** CNC-25f composite membrane, **c** CNC-250f composite membrane, **d** Statistical roughness measurements of RMS for 5 individual measurements of each sample, **e** Zeta potential of CNC-25f and CNC-250f, **f** the permeation flux (F) of composite membrane of neat MCA, CNC-250f@0.35, CNC-250f@1.06, CNC-250f@3.53 and CNC-250f@10.6, respectively

Elemental mapping analysis also indicates the successful fabrication of CNC composite membranes as shown in Fig. 7i–l. The neat MCA membrane show C, N and O element signals. With increasing the loading contents of CNC, the characteristic S element appeared (insets in Fig. 7j–l) due to the existence of sulfate groups in CNCs.

4 Conclusion

Two different aspect ratios of the CNCs prepared from different MCCs were obtained through sulfur acid hydrolysis via pre-frozen method. Among them, the CNC-25f bears the smaller aspect ratio of 10.7, while CNC-250f is slenderer with that of 34.8. Both of the CNC samples show similar nanowhisker morphology with a dimension of (150–300 nm in length) × (8–15 nm in width). The nanowhisker morphology, crystalline index and Iβ structure of obtained CNCs was confirmed by TEM/AFM, XRD and FTIR, respectively. The thermal stability showed 40% of weight lost in the first 130–240 °C region and further decomposed to 30% residual with further increasing temperature up to 700 °C. Furthermore, such CNC samples can be fabricated into nano-composite membrane, and the permeation flux of the membrane is CNC-concentration dependent. The CNC-250f with higher AR value serves as a promising candidate, which facilitates its application in effective cationic dye removal, i.e. 99.9% removal of Methylene Blue at 10 mg/L and 97.9% removal of Rhodamine B at 20 mg/L at an optimum concentration of CNC-250f@10.6 mg/mL with the MCA as the substrate. Such effect is due to the steric hindering and electrostatic interaction between the anionic CNCs composite membranes and cationic dyes.

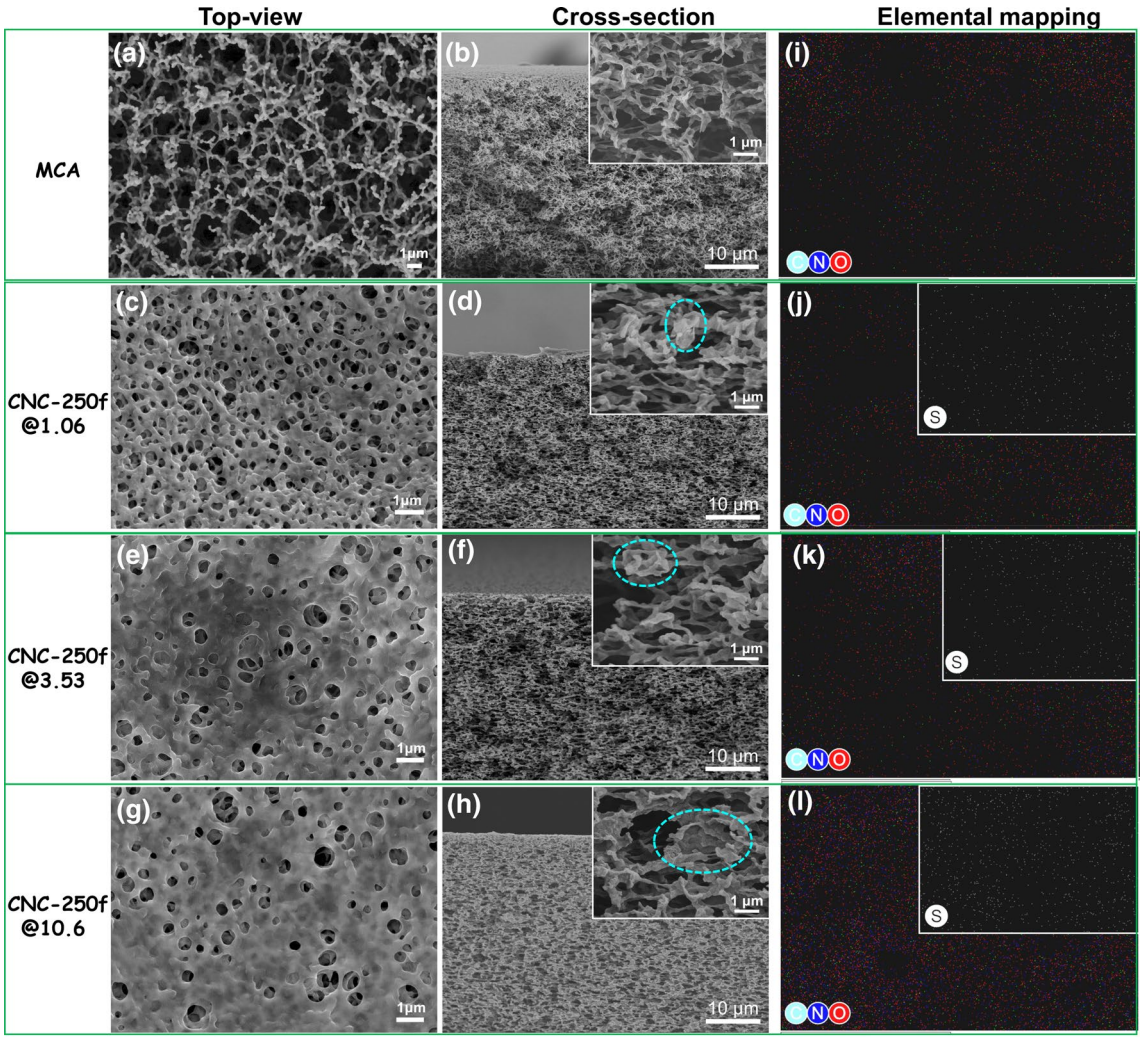

Fig. 7 SEM images of the top-view and cross-sectional morphology and elemental mapping of neat MCA membrane (**a**, **b**, **i**), CNC-250f@1.06 (**c**, **d**, **j**), CNC-250f@3.53 (**e**, **f**, **k**) and CNC-250f@10.6 (**g**, **h**, **l**) composite membranes, respectively

Acknowledgements This research was financially supported by the Tianjin Science and Technology Major Project Program (18ZXJMTG00070).

Compliance with ethical standards

Conflict of interest The authors declare that they have no competing interest.

References

1. Chen W, Yu H, Lee S-YY et al (2018) Nanocellulose: a promising nanomaterial for advanced electrochemical energy storage. Chem Soc Rev 47:2837–2872. https://doi.org/10.1039/C7CS00790F
2. Seabra AB, Bernardes JS, Fávaro WJ et al (2018) Cellulose nanocrystals as carriers in medicine and their toxicities: a review. Carbohydr Polym 181:514–527. https://doi.org/10.1016/j.carbpol.2017.12.014
3. Wang N, Ouyang XK, Yang LY, Omer AM (2017) Fabrication of a magnetic cellulose nanocrystal/metal-organic framework composite for removal of Pb(II) from water. ACS Sustain Chem Eng 5:10447–10458. https://doi.org/10.1021/acssuschemeng.7b02472
4. Pattinson SW, Hart AJ (2017) Additive manufacturing of cellulosic materials with robust mechanics and antimicrobial functionality. Adv Mater Technol 2:1600084. https://doi.org/10.1002/admt.201600084
5. Sehaqui H, Ezekiel Mushi N, Morimune S et al (2012) Cellulose nanofiber orientation in nanopaper and nanocomposites by cold drawing. ACS Appl Mater Interfaces 4:1043–1049. https://doi.org/10.1021/am2016766
6. Corrêa AC, de Teixeira EM, Pessan LA, Mattoso LHC (2010) Cellulose nanofibers from curaua fibers. Cellulose 17:1183–1192. https://doi.org/10.1007/s10570-010-9453-3
7. Jiang F, Esker AR, Roman M (2010) Acid-catalyzed and solvolytic desulfation of H_2SO_4-hydrolyzed cellulose nanocrystals. Langmuir 26:17919–17925. https://doi.org/10.1021/la1028405

8. Tang L, Huang B, Lu Q et al (2013) Ultrasonication-assisted manufacture of cellulose nanocrystals esterified with acetic acid. Bioresour Technol 127:100–105. https://doi.org/10.1016/j.biortech.2012.09.133
9. Cheng F, Liu C, Wei X et al (2017) Preparation and characterization of 2,2,6,6-tetramethylpiperidine-1-oxyl (TEMPO)-oxidized cellulose nanocrystal/alginate biodegradable composite dressing for hemostasis applications. ACS Sustain Chem Eng 5:3819–3828. https://doi.org/10.1021/acssuschemeng.6b02849
10. Leung ACW, Hrapovic S, Lam E et al (2011) Characteristics and properties of carboxylated cellulose nanocrystals prepared from a novel one-step procedure. Small 7:302–305. https://doi.org/10.1002/smll.201001715
11. de Campos A, Correa AC, Cannella D et al (2013) Obtaining nanofibers from curaua and sugarcane bagasse fibers using enzymatic hydrolysis followed by sonication. Cellulose 20:1491–1500. https://doi.org/10.1007/s10570-013-9909-3
12. Kang X, Kuga S, Wang C et al (2018) Green preparation of cellulose nanocrystal and its application. ACS Sustain Chem Eng 6:2954–2960. https://doi.org/10.1021/acssuschemeng.7b02363
13. Habibi Y, Lucia LA, Rojas OJ (2010) Cellulose nanocrystals: chemistry, self-assembly, and applications. Chem Rev 110:3479–3500. https://doi.org/10.1021/cr900339w
14. Rosa MF, Medeiros ES, Malmonge JA et al (2010) Cellulose nanowhiskers from coconut husk fibers: effect of preparation conditions on their thermal and morphological behavior. Carbohydr Polym 81:83–92. https://doi.org/10.1016/j.carbpol.2010.01.059
15. Sun X, Wu Q, Ren S, Lei T (2015) Comparison of highly transparent all-cellulose nanopaper prepared using sulfuric acid and TEMPO-mediated oxidation methods. Cellulose 22:1123–1133. https://doi.org/10.1007/s10570-015-0574-6
16. Habibi Y, Chanzy H, Vignon MR (2006) TEMPO-mediated surface oxidation of cellulose whiskers. Cellulose 13:679–687. https://doi.org/10.1007/s10570-006-9075-y
17. Lagerwall JPFF, Schütz C, Salajkova M et al (2014) Cellulose nanocrystal-based materials: from liquid crystal self-assembly and glass formation to multifunctional thin films. NPG Asia Mater 6:e80. https://doi.org/10.1038/am.2013.69
18. Wang N, Ding E, Cheng R (2007) Thermal degradation behaviors of spherical cellulose nanocrystals with sulfate groups. Polymer (Guildf) 48:3486–3493. https://doi.org/10.1016/j.polymer.2007.03.062
19. Kalashnikova I, Bizot H, Bertoncini P et al (2013) Cellulosic nanorods of various aspect ratios for oil in water Pickering emulsions. Soft Matter 9:952–959. https://doi.org/10.1039/C2SM26472B
20. Rajendran S, Khan MM, Gracia F et al (2016) Ce^{3+}-ion-induced visible-light photocatalytic degradation and electrochemical activity of ZnO/CeO_2 nanocomposite. Sci Rep 6:1–11. https://doi.org/10.1038/srep31641
21. Şen F, Demirbaş Ö, Çalımlı MH et al (2018) The dye removal from aqueous solution using polymer composite films. Appl Water Sci 8:206. https://doi.org/10.1007/s13201-018-0856-x
22. Forgacs E, Cserháti T, Oros G (2004) Removal of synthetic dyes from wastewaters: a review. Environ Int 30:953–971. https://doi.org/10.1016/j.envint.2004.02.001
23. Mahmoud ME, Nabil GM, El-Mallah NM, Karar SB (2016) Assessment of the adsorptive color removal of methylene blue dye from water by activated carbon sorbent-immobilized-sodium decyl sulfate surfactant. Desalination Water Treat 57:8389–8405. https://doi.org/10.1080/19443994.2015.1019367
24. Mahmoud ME, Nabil GM, Khalifa MA, El-Mallah NM, Hassouba HM (2019) Effective removal of crystal violet and methylene blue dyes from water by surface functionalized zirconium silicate nanocomposite. J Environ Chem Eng 7:103009. https://doi.org/10.1016/j.jece.2019.103009
25. Ghaee A, Shariaty-Niassar M, Barzin J et al (2016) Preparation of chitosan/cellulose acetate composite nanofiltration membrane for wastewater treatment. Desalination Water Treat 57:14453–14460. https://doi.org/10.1080/19443994.2015.1068228
26. He Y, Li GM, Wang H et al (2009) Experimental study on the rejection of salt and dye with cellulose acetate nanofiltration membrane. J Taiwan Inst Chem Eng 40:289–295. https://doi.org/10.1016/j.jtice.2008.08.008
27. Boricha AG, Murthy ZVP (2010) Preparation of N, O-carboxymethyl chitosan/cellulose acetate blend nanofiltration membrane and testing its performance in treating industrial wastewater. Chem Eng J 157:393–400. https://doi.org/10.1016/j.cej.2009.11.025
28. Gupta VK, Suhas (2009) Application of low-cost adsorbents for dye removal—a review. J Environ Manag 90:2313–2342. https://doi.org/10.1016/j.jenvman.2008.11.017
29. Huang Z-M, Zhang Y, Kotaki M, Ramakrishna S (2003) A review on polymer nanofibers by electrospinning and their applications in nanocomposites. Compos Sci Technol 63:2223–2253. https://doi.org/10.1016/S0266-3538(03)00178-7
30. Anglès MN, Dufresne A (2001) Plasticized starch/tunicin whiskers nanocomposite materials. 2. Mechanical behavior. Macromolecules 34:2921–2931. https://doi.org/10.1021/ma001555h
31. Azizi Samir MAS, Alloin F, Dufresne A (2005) Review of recent research into cellulose whiskers, their properties and their application in nanocomposite field. Biomacromolecules 6:612–626. https://doi.org/10.1021/bm0493685
32. Oksman K, Etang JA, Mathew AP, Jonoobi M (2011) Cellulose nanowhiskers separated from a bio-residue from wood bioethanol production. Biomass Bioenergy 35:146–152. https://doi.org/10.1016/j.biombioe.2010.08.021
33. Segal L, Creely JJ, Martin AE, Conrad CM (1959) An empirical method for estimating the degree of crystallinity of native cellulose using the X-Ray diffractometer. Text Res J 29:786–794. https://doi.org/10.1177/004051755902901003
34. Yu H, Qin Z, Liang B et al (2013) Facile extraction of thermally stable cellulose nanocrystals with a high yield of 93% through hydrochloric acid hydrolysis under hydrothermal conditions. J Mater Chem A 1:3938–3944. https://doi.org/10.1039/c3ta01150j
35. Shi H, Li W, Zhong L, Xu C (2014) Methylene blue adsorption from aqueous solution by magnetic cellulose/graphene oxide composite: equilibrium, kinetics, and thermodynamics. Ind Eng Chem Res 53:1108–1118. https://doi.org/10.1021/ie4027154
36. Cherian BM, Pothan LA, Nguyen-Chung T et al (2008) A novel method for the synthesis of cellulose nanofibril whiskers from banana fibers and characterization. J Agric Food Chem 56:5617–5627. https://doi.org/10.1021/jf8003674
37. Lu P, Lo Hsieh Y (2010) Preparation and properties of cellulose nanocrystals: rods, spheres, and network. Carbohydr Polym 82:329–336. https://doi.org/10.1016/j.carbpol.2010.04.073
38. Azzaoui K, Lamhamdi A, Mejdoubi EM et al (2014) Synthesis and characterization of composite based on cellulose acetate and hydroxyapatite application to the absorption of harmful substances. Carbohydr Polym 111:41–46. https://doi.org/10.1016/j.carbpol.2014.04.058
39. George J, Ramana KV, Bawa AS, Siddaramaiah (2011) Bacterial cellulose nanocrystals exhibiting high thermal stability and their polymer nanocomposites. Int J Biol Macromol 48:50–57. https://doi.org/10.1016/j.ijbiomac.2010.09.013
40. Roman M, Winter WT (2004) Effect of sulfate groups from sulfuric acid hydrolysis on the thermal degradation behavior of bacterial cellulose. Biomacromolecules 5:1671–1677. https://doi.org/10.1021/bm034519+

41. Boussu K, Van der Bruggen B, Volodin A et al (2005) Roughness and hydrophobicity studies of nanofiltration membranes using different modes of AFM. J Colloid Interface Sci 286:632–638. https://doi.org/10.1016/j.jcis.2005.01.095
42. Karim Z, Mathew AP, Grahn M et al (2014) Nanoporous membranes with cellulose nanocrystals as functional entity in chitosan: removal of dyes from water. Carbohydr Polym 112:668–676. https://doi.org/10.1016/j.carbpol.2014.06.048
43. Yang HY, Han ZJ, Yu SF et al (2013) Carbon nanotube membranes with ultrahigh specific adsorption capacity for water desalination and purification. Nat Commun 4:2220–2228. https://doi.org/10.1038/ncomms3220